



RESEARCH LETTER

10.1002/2014GL061637

Key Points:

- Ocean dye releases were mapped using scanning, depth-resolving airborne lidar
- Dye evolved into rolls aligned with the wind and/or near-surface current
- Large-eddy simulations showed similar features without Stokes drift forcing

Correspondence to:

M. A. Sundermeyer,
msundermeyer@umassd.edu

Citation:

Sundermeyer, M. A., E. Skillingstad, J. R. Ledwell, B. Concannon, E. A. Terray, D. Birch, S. D. Pierce, and B. Cervantes (2014), Observations and numerical simulations of large-eddy circulation in the ocean surface mixed layer, *Geophys. Res. Lett.*, 41, 7584–7590, doi:10.1002/2014GL061637.

Received 26 AUG 2014

Accepted 14 OCT 2014

Accepted article online 17 OCT 2014

Published online 6 NOV 2014

Observations and numerical simulations of large-eddy circulation in the ocean surface mixed layer

Miles A. Sundermeyer¹, Eric Skillingstad², James R. Ledwell³, Brian Concannon⁴, Eugene A. Terray³, Daniel Birch¹, Stephen D. Pierce², and Brandy Cervantes²

¹School for Marine Science and Technology, University of Massachusetts Dartmouth, North Dartmouth, Massachusetts, USA, ²College of Earth, Ocean, and Atmospheric Sciences, Oregon State University, Corvallis, Oregon, USA, ³Woods Hole Oceanographic Institution, Woods Hole, Massachusetts, USA, ⁴Naval Air Systems Command, Patuxent River, Maryland, USA

Abstract Two near-surface dye releases were mapped on scales of minutes to hours temporally, meters to order 1 km horizontally, and 1–20 m vertically using a scanning, depth-resolving airborne lidar. In both cases, dye evolved into a series of rolls with their major axes approximately aligned with the wind and/or near-surface current. In both cases, roll spacing was also of order 5–10 times the mixed layer depth, considerably larger than the 1–2 aspect ratio expected for Langmuir cells. Numerical large-eddy simulations under similar forcing showed similar features, even without Stokes drift forcing. In one case, inertial shear driven by light winds induced large aspect ratio large-eddy circulation. In the second, a preexisting lateral mixed layer density gradient provided the dominant forcing. In both cases, the growth of the large-eddy structures and the strength of the resulting dispersion were highly dependent on the type of forcing.

1. Introduction

Accurate representation of the surface ocean boundary layer is key to understanding the coupled ocean-atmosphere system. Exchange at the air-sea interface is in part controlled by mixing processes in the ocean boundary layer (OBL). Consequently, understanding such processes is crucial to accurately portraying ocean forcing by winds and air-sea interactions that control weather and climate.

Surface wind and wave forcing are responsible for the bulk of turbulent mixing processes active in the OBL through the formation of large-eddy circulation, including Langmuir circulation and other shear-generated instabilities. Large-eddy circulations in the OBL have been shown by numerous investigators to enhance upper ocean mixing through the efficient transport of momentum and heat [e.g., *Smith, 1992; Skillingstad and Denbo, 1995; Li and Garrett, 1997; Kukulka et al., 2009*]. In low wind, convection can dominate mixing during strong surface cooling. Such processes have been observed [e.g., *Shay and Gregg, 1986; Plueddemann et al., 1996*] as well as modeled [e.g., *Skillingstad and Denbo, 1995; McWilliams et al., 1997*] with generally good agreement [*Kukulka et al., 2010*]. More recent studies have focused on the various roles of surface wave breaking [*Melville and Matusov, 2002; Sullivan et al., 2007*], wave direction [*Van Roekel et al., 2012*] and tidal flow interactions [*Kukulka et al., 2011*].

As our understanding of large-eddy circulation in the OBL has evolved, it is now recognized that what has historically been generically termed “Langmuir circulation” actually consists of a variety of instability phenomena, including classic Langmuir circulation, convective turbulence in the presence of shear, and/or inflection point, parallel, and symmetric instabilities [e.g., *Thorpe, 2004*]. Separating one instability mechanism from another is still a major challenge, as numerous parameters and forcings drive the various instabilities, including sea state (from fetch-limited to fully developed seas to nonlocally forced swell), surface buoyancy flux (positive and negative), lateral buoyancy gradients, and ranges of angles between the wind, currents, and waves, to name a few.

While some progress has been made differentiating regimes of one type of instability over another [e.g., *Li et al., 2005*] and parameterizing the resulting mixing and/or OBL deepening under specific circumstances [e.g., *Li and Garrett, 1997*], there are still many open questions as to how various theoretical instabilities manifest and/or compete under real ocean conditions. Wind rows and/or surface thermal structure from infrared imaging have long revealed patterns of surface convergence [e.g., *Langmuir, 1938; Marmorino et al., 2005*]. Pioneering observations of *Weller et al.* [1985] revealed the three-dimensional

structure of Langmuir circulation in the open ocean. Acoustic measurements of bubble clouds have further provided direct evidence of downwelling circulations and their horizontal scales [e.g., Farmer and Li, 1995; Plueddemann *et al.*, 1996]. In addition, advances in observational technologies and computational power have enabled numerous large-eddy simulation (LES) studies to at least qualitatively reproduce the observations.

We report here on results from two dye release experiments conducted in the OBL during summertime fair-weather forcing conditions and accompanying numerical simulations aimed at diagnosing the underlying physical processes driving the observed dye evolution. A key aspect of this work is the combination of high-resolution (time and space) measurements of dye dispersion in the OBL combined with realistic LES simulations of upper ocean boundary layer dynamics.

2. Methods

The first dye experiment we report here was conducted on 3 June 2004 off the east coast of Florida, in approximately 200 m of water, 5 km east of Fort Lauderdale. The study site was offshore enough to be outside the nearshore band of higher chlorophyll, but not so far as to be within the stronger currents associated with the Gulf Stream. A solution of 5 kg of rhodamine dye mixed with isopropyl alcohol and seawater so as to be approximately neutrally buoyant was injected in the near surface of the ocean at ~09:00 h local time. During the injection, the depth of the injection sled was varied in a stair-step fashion beginning with a segment at 2.5 m for ~1 min, followed by a deeper segment at 5 m, followed by an even deeper segment at 10 m, then returning to the surface and repeating. The result was a series of surface segments, interspersed with progressively deeper segments at discrete depths. The complete injection lasted approximately 15 min, resulting in an injection streak ~1600 m long.

The second dye experiment was conducted on 16 June 2011 in the Sargasso Sea east of North Carolina, in approximately 4000 m of water, 250 km east of Cape Hatteras. In this case, the study site was offshore of the Gulf Stream in a region of open ocean mesoscale and submesoscale eddy and frontal activity. A solution of 9 kg of fluorescein dye mixed with isopropyl alcohol and seawater was injected in the near surface at approximately 01:00 h local time. In this experiment the injection sled was maintained at 2.3 m depth for a total injection time of 4 min, resulting in an injection streak length of ~0.13 km.

In both experiments, dye distributions were sampled using a conductivity-temperature-depth (CTD)/fluorometer instrument package towed behind the ship, together with airborne lidar. Shipboard acoustic Doppler current profilers (ADCPs) were used to measure ocean currents in and around the dye patches. Wind observations for the 2004 experiment were obtained from nearby Fort Lauderdale airport, while for the 2011 experiment they were measured from a meteorological package mounted on the ship.

The use of airborne lidar to survey the dye patches is a significant novel component of the experiments reported here. For the 2004 experiment, we used a SHOALS-1000 T lidar manufactured by Optech Inc. and operated by the U.S. Army Corps of Engineers Joint Airborne Lidar Bathymetry Technical Center of Expertise. The system uses a frequency-doubled neodymium: yttrium/aluminum/garnet laser to produce 1064 (infrared) and 532 nm (green) pulses 6 ns in duration, with a repetition rate of 1 kHz and a scan rate transverse to the direction of flight of 10–15 Hz. Excitation at 532 nm is approximately one half peak excitation (at 555 nm) for rhodamine-WT dye used in the 2004 experiments. Further details of the experiment are reported in Sundermeyer *et al.* [2007].

For the 2011 experiment, we used a lidar built and designed by the Naval Air Systems Command. The system uses a Ti:Sapphire tunable laser set to 480 nm, with a pulse length of 10 ns, a repetition rate of 1 kHz and a conical scan rate of 15 Hz. Excitation at 480 nm is approximately three fourths peak excitation (at 490 nm) for fluorescein dye used in the 2011 experiments. Details of the 2011 field experiments will be reported in a forthcoming manuscript.

In both the 2004 and 2011 experiments, lidar data were georeferenced using the aircraft inertial navigation system and translated into an advected reference frame by integrating the velocity from the shipboard ADCP. An inversion algorithm to convert the lidar returns to absolute dye concentration was applied to the 2004 data and is reported by Sundermeyer *et al.* [2007]. A second generation inversion routine for the 2011 data is in preparation. However, for brevity, we report here simply the intensity and depth of the peak

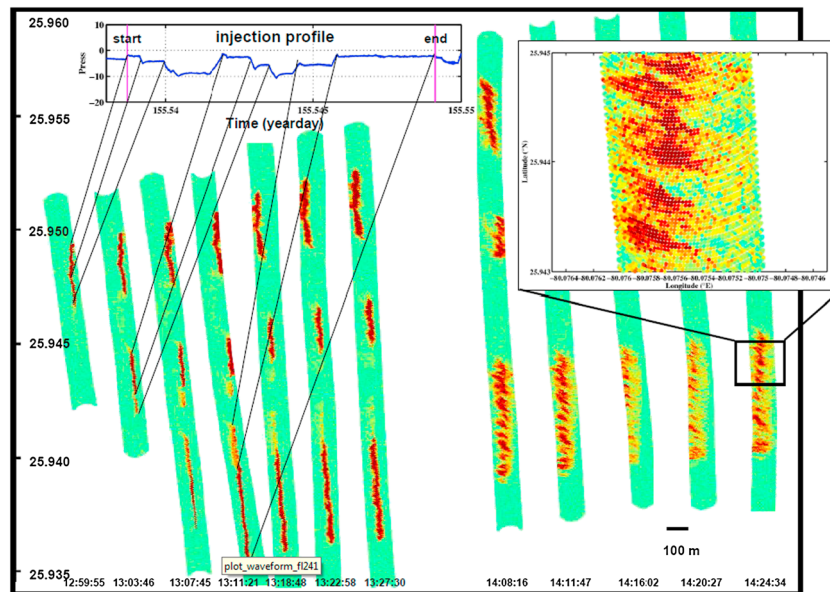


Figure 1. Successive lidar flight lines from June 2004 dye release ordered by time from left to right [after Terray *et al.*, 2005]. Color indicates peak lidar fluorescence for each waveform. Y axis is latitude, with successive flight lines offset left to right for clarity. Times at base of figure correspond to start of each flight line, with a gap from 13:27–14:08 h during a period when flight lines were east-west rather than north-south (not shown). Top inset shows pressure record during ~15 min long injection with changes in injection depth as indicated.

returns of the lidar, which, together with in situ dye fluorometer observations, provide sufficient insight into the underlying physics.

Numerical simulations corresponding to the two experimental scenarios were conducted using the LES model described in *Skyllingstad et al.* [2000]. The model is based on the incompressible, nonhydrostatic, rotating f plane, Boussinesq equations with subgrid turbulence parameterization following *Ducros et al.* [1996]. Periodic lateral boundaries are employed, with rigid upper and lower boundaries and a sponge layer at the model bottom to absorb vertically propagating internal waves. Surface wave effects are parameterized using the *Craik and Leibovich* [1976] Stokes drift vortex forcing term with a representative monochromatic wave system aligned with the mean wind.

3. Results

3.1. The 2004 Experiment

Conditions during the 2004 rhodamine experiment were generally fair for the week prior to as well as during the experiment, except for occasional thunderstorms in the area during afternoon/evening hours. Meteorological data were not available from the ship; however, data collected at the nearby Fort Lauderdale airport were generally consistent with conditions observed at the study site, namely, scattered to partly cloudy with winds generally less than 10 kts out of the southeast. Wave heights throughout the experiment were of order 0.5 m or less. CTD data collected during the dye surveys showed a strongly stratified surface layer ($N \sim 10$ cph) extending to about 10 m, overlying a less stratified region down to 35 m ($N \sim 3.5$ cph), followed by an abrupt density jump (approximately 0.5 kg m^{-3}) at 35 m, consistent with a remnant mixed layer capped by surface heating (not shown). If there was a surface mixed layer, it was confined to the upper 2–3 m where the towed CTD/fluorometer system was unable to resolve it. Mean currents were approximately 10 cm s^{-1} northward near the surface, with a 25 cm s^{-1} NW subsurface maximum centered around 10 m, and a return to northward flow below 20 m of $15\text{--}20 \text{ cm s}^{-1}$, that is, with a near-surface shear in the upper 10 m opposing the wind.

Airborne lidar surveys were conducted for ~ 1.5 h beginning at the start of the dye injection. A summary of the dye overflights is shown in Figure 1. Results show the surface segments of the patch evolved into a banded structure oriented approximately in the direction of the wind, with a dominant length scale in the crosswind direction of 40–50 m by the end of the surveys. Notable here is that classic Langmuir circulation typically has aspect ratios of

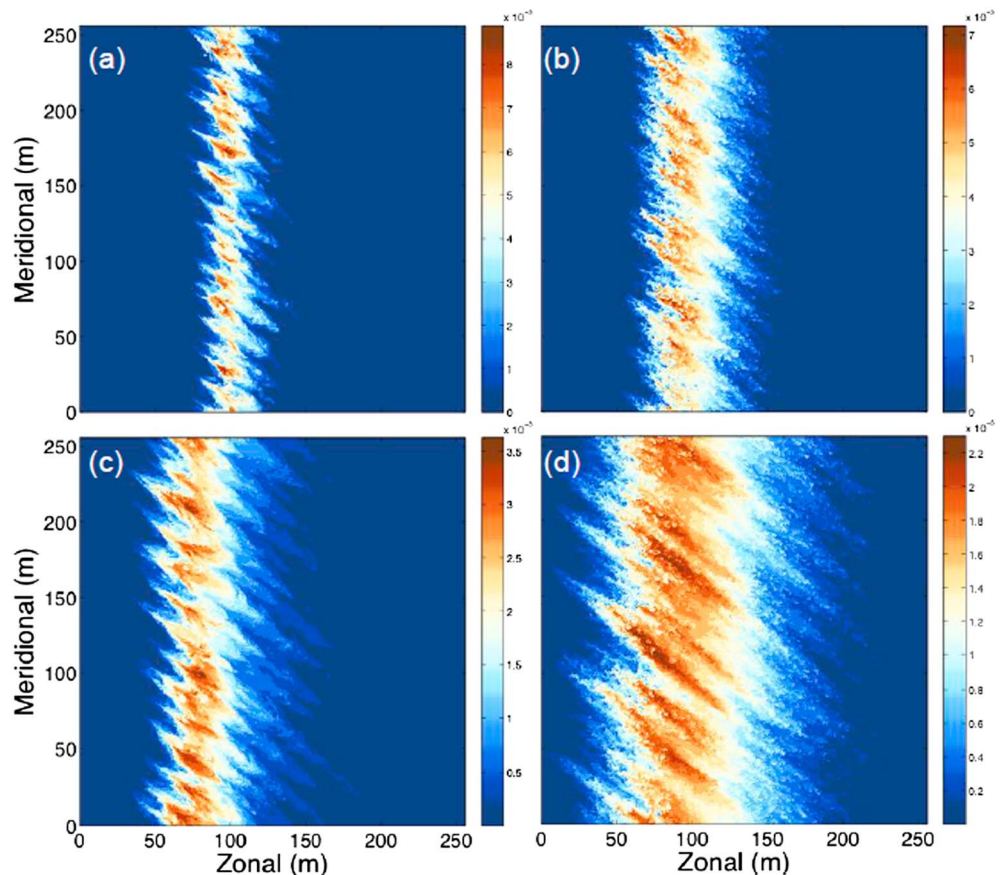


Figure 2. Normalized dye concentrations (a, c) 0.5 and (b, d) 1.0 h after release using parameters similar to 2004 lidar dye observations shown in Figure 1 for Figures 2a and 2b Stokes drift and wind stress forcing and Figures 2c and 2d wind stress-only forcing. Wind stress = 0.05 N/m^{-2} , surface wave length = 15 m, wave height = 0.5 m, wind/wave direction from 120° .

order 1–2 (cell spacing to mixed layer, ML, depth). However, as we estimate the mixed layer depth for this experiment was not more than 2–3 m, the 40–50 m spacing of the observed roll structures was much larger than would be explained by this mechanism. Further, the direction of the mean shear in the upper 3–10 m opposed the wind, suggesting the presence of either residual inertial shear, or of a lateral density gradient driving near-surface flow. Either of these factors alone could equally explain the observed large-eddy structures.

To better understand the underlying physics, LES model runs were forced with conditions similar to those observed. The model was started at rest using an idealized temperature profile with a 2 m deep surface mixed layer above a thermocline gradient of 1°C per 8 m depth. Wind forcing of 0.05 N m^{-2} was applied along with a Stokes drift profile representing a monochromatic surface wave with amplitude 0.5 m and wavelength of 15 m. Simulations were conducted for 4 h with the initial 2 h considered a spin-up period before releasing a passive surface tracer in a north-south line 1 m wide at the center of the domain at a depth of 0.5 m.

Two cases were considered, one with Stokes drift forcing and hence classic Langmuir circulation and a second with Stokes drift removed, representing mainly wind-driven shear flow. Normalized dye concentration for each case after 30 and 60 min (Figure 2) show that both cases generate banded structures with spacing similar to the dye observations. This similarity between these two cases suggests that ML shear (associated with wind-driven inertial oscillations in the case of the model) is equally capable of generating large-eddy circulations given the observed stratification. The main difference between the two cases is the markedly larger horizontal mixing in the case without Stokes drift. The cause of this greater horizontal transport is the much higher mixed layer shear when Langmuir circulation is not present, an effect previously noted by *Skyllingstad et al.* [1999]. In one case the Stokes drift forcing term and resulting Langmuir circulations act to homogenize shear in the mixed layer, whereas without Langmuir circulation, surface currents increase rapidly

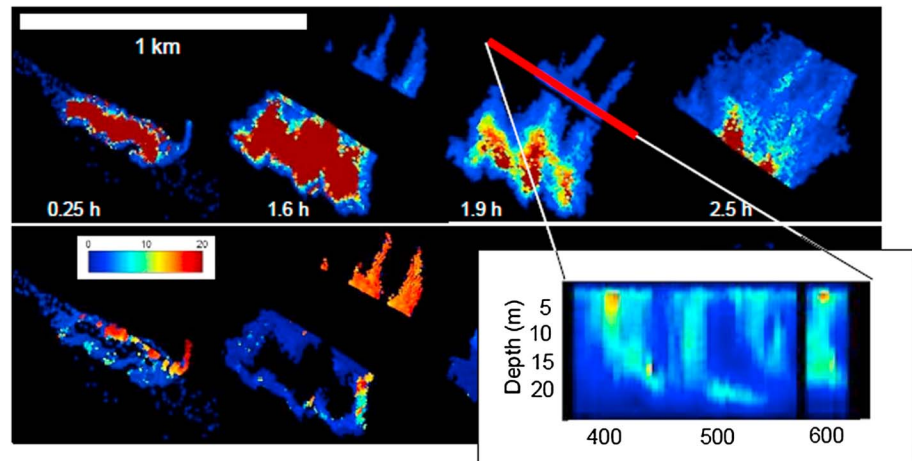


Figure 3. Evolution of a near-surface (3 m) fluorescein dye patch as viewed by airborne lidar during the 2011 LatMix field experiment. (top row) Peak lidar fluorescence intensity during successive surveys with time (indicated under each patch, hours) increasing from left to right. (bottom) The depth at which the peak return was observed. Wind was from the north at ~13 kts. There was also a mean density gradient within the ML oriented roughly NW-SE. Bottom right inset shows a depth cross section of the lidar return (marked by red line in Figure 3 (top)), revealing deep tails (i.e., at the ML base) streaming behind (relative to the wind direction) the surface portion of the patch.

in response to the wind until turbulence produced by shear balances the momentum flux. A key difference between the two numerical simulations is thus that differential transport of dye by the sheared current combined with vertical mixing generates more rapid lateral mixing. Other than this overall increase in mixing, however, it is difficult to discern a difference in character between the two modeled dye patterns.

3.2. The 2011 Experiment

Conditions during the 2011 fluorescein experiment were again relatively fair for the period leading up to and during the experiment. Mean wind was 13 kts from the north (354°), with wave heights typically ~2 m or less. CTD data collected during the dye surveys showed a surface mixed layer depth of ~15 m, deepening to ~18 m by the end of the experiment. Mean current was approximately 40 cm s^{-1} WNW at the surface, with a 50 cm s^{-1} NNW subsurface maximum centered at about 25 m and a return to $\sim 40 \text{ cm s}^{-1}$ WNW below 40 m; that is, current largely opposing the wind but with a down and slightly to the right of the wind near-surface shear.

In this experiment, airborne lidar surveys were conducted for ~2.5 h following the injection. A summary of the dye surveys is shown in Figure 3. Again, clear roll structures were evident in the dye distributions within 15 min following the injection (note that repeat lidar surveys were more sparse in this experiment, since the aircraft spent some of its time surveying another deeper dye release north of the surface patch). Again, the observed roll structures were oriented roughly downwind, this time with a dominant crosswind length scale of order 150 m. Once again, we note the large horizontal scale of the rolls compared to the ML depth. Also notable is that although the observed roll structures were roughly aligned with the wind, they also displayed distinct tails at the ML base. That is, despite the dye injected near the surface being rapidly mixed down to the ML base (the 0.25 h snapshot in Figure 3 already shows dye at 20 m depth), the streamers at the ML base were apparently not equally rapidly mixed back up through the ML.

LES simulations were again conducted with wind and wave forcing similar to that observed. In contrast to the previous case, however, a background front was imposed with a geostrophic shear based on an estimated horizontal temperature gradient of $0.1^\circ\text{C km}^{-1}$ as measured by the ship injecting the dye. In this simulation, mixed layer circulations were strongly affected by the frontal system, with coherent rolls produced at horizontal scales of 150–200 m or about 10–15 times the mixed layer depth. Here the model dye patch (Figure 4) formed coherent structures of similar scale regardless of the Stokes drift forcing. By contrast, without the front the dye organized into patches of much smaller scale, more similar to the Florida scenario. Also evident in the frontal simulations were distinct tails at the ML base associated with dye that had been mixed isopycnally down and into the vertically stratified region below the ML.

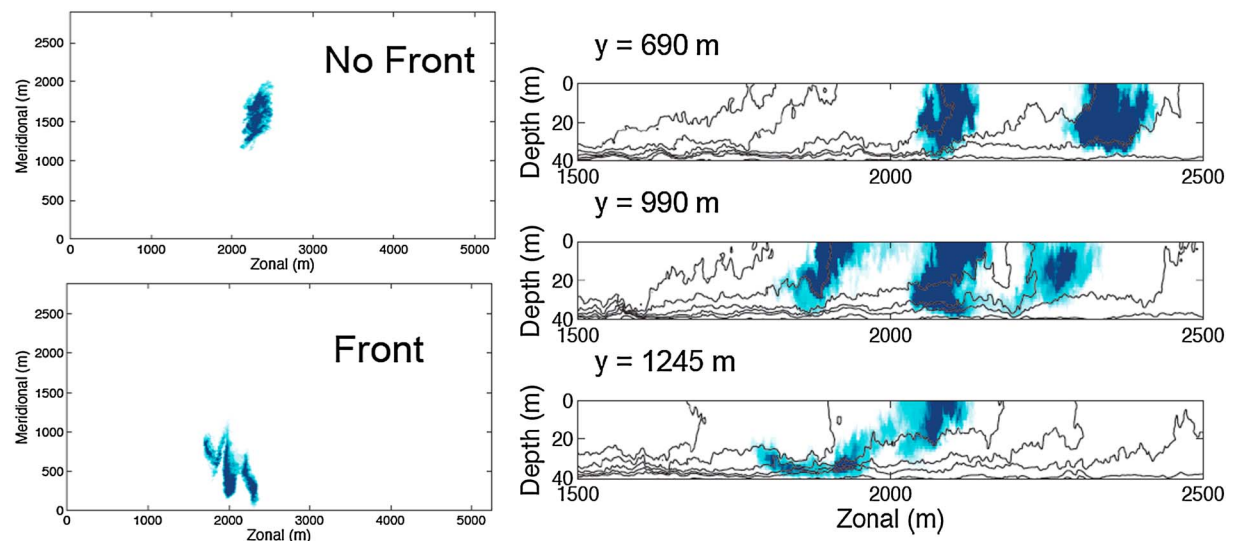


Figure 4. Normalized dye streaks from numerical simulations using parameters similar to the 2011 lidar dye observations shown in Figure 3, (left column) without and with a background ML density gradient. (right column) Transects of density (black contours) and dye (color) at various positions upstream/downstream of the surface dye expression for the ML front case. Note the tails of dye penetrating the stable stratification below the ML, reminiscent of the observations shown in Figure 3.

4. Discussion/Conclusions

Field observations of dye dispersion using airborne lidar reveal a rich structure of large-eddy circulations in the OBL. Simulations of two dye cases suggest that multiple mechanisms can lead to coherent, banded dye structures in the ocean mixed layer. The growth of these structures and hence the strength of the associated dispersion, for a given boundary layer depth, are highly dependent on the type of forcing. For example, in the case of waves and wind-driven mixing, Stokes drift forcing acts to decrease shear dispersion resulting in slower spreading of the dye plume and smaller coherent structures. Frontal instabilities, on the other hand, generate banded structures with lateral separations many times the mixed layer depth, which rapidly pull the dye patch apart into discrete elements with scales much larger than are produced by shear or wave-induced circulations. The combination of high-resolution (both in time and space) field observations together with process-driven numerical simulations provide a valuable tool for diagnosing which of these (among other processes) might dominate under different forcing conditions.

Acknowledgments

Support for the 2004 field experiment was provided by the Cecil H. and Ida M. Green Technology Innovation Fund and Coastal Ocean Institute grant 27001545, both through Woods Hole Oceanographic Institution, and by Office of Naval Research grant N00014-01-1-0984. Support for the 2011 field experiments was provided by ONR grants N00014-09-1-0194, N00014-09-1-0175, N00014-11-WX-21010, N00014-12-WX-21031, and N00014-09-1-0460 and NSF grants OCE-0751734 and OCE-0751653. Simulations were supported under grant N00014-09-1-0268. Lidar data represented in Figures 1 and 3 can be obtained by contacting M. Sundermeyer. Numerical model results depicted in Figures 2 and 4 can be obtained by contacting E. Skillingstad. In memoriam Murray Levine.

Lisa Beal thanks two anonymous reviewers for their assistance in evaluating this paper.

References

- Craik, A. D. D., and S. Leibovich (1976), A rational model for Langmuir circulations, *J. Fluid Mech.*, *73*(3), 401–426.
- Ducros, F., P. Comte, and M. Lesieur (1996), Large-eddy simulation of transition to turbulence in a boundary layer developing spatially over a flat plate, *J. Fluid Mech.*, *326*, 1–36.
- Farmer, D., and M. Li (1995), Patterns of bubble clouds organized by Langmuir circulation, *J. Phys. Oceanogr.*, *25*(6), 1426–1440.
- Kukulka, T., A. J. Plueddemann, J. H. Trowbridge, and P. P. Sullivan (2009), Significance of Langmuir circulations in upper ocean mixing: A comparison between observations and large eddy simulations, *Geophys. Res. Lett.*, *36*, L10603, doi:10.1029/2009GL03762.
- Kukulka, T., A. J. Plueddemann, J. H. Trowbridge, and P. P. Sullivan (2010), Rapid mixed layer deepening by the combination of Langmuir and shear instabilities—A case study, *J. Phys. Oceanogr.*, *40*(11), 2381–2400.
- Kukulka, T., A. J. Plueddemann, J. H. Trowbridge, and P. P. Sullivan (2011), The influence of crosswind tidal currents on Langmuir circulation in a shallow ocean, *J. Geophys. Res.*, *116*, C08005, doi:10.1029/2011JC006971.
- Langmuir, I. (1938), Surface motion of water induced by wind, *Science*, *87*, 119–23.
- Li, M., and C. Garrett (1997), Mixed layer deepening due to Langmuir circulation, *J. Phys. Oceanogr.*, *27*, 121–132.
- Li, M., C. Garrett, and E. Skillingstad (2005), A regime diagram for classifying turbulent large eddies in the upper ocean, *Deep Sea Res. I*, *52*, 259–78.
- Marmorino, G. O., G. B. Smith, and G. J. Lindemann (2005), Infrared imagery of large-aspect-ratio Langmuir circulation, *Cont. Shelf Res.*, *25*(1), 1–6.
- McWilliams, J. C., P. P. Sullivan, and C. H. Moeng (1997), Langmuir turbulence in the ocean, *J. Fluid Mech.*, *334*, 1–30.
- Melville, W. K., and P. Matusov (2002), Distribution of breaking waves at the ocean surface, *Nature*, *417*, 58–63.
- Plueddemann, A., J. Smith, D. Farmer, R. Weller, W. Crawford, R. Pinkel, S. Vagle, and A. Gnanadesikan (1996), Structure and variability of Langmuir circulation during the surface waves processes program, *J. Geophys. Res.*, *101*(C2), 3525–3543, doi:10.1029/95JC03282.
- Shay, T. J., and M. C. Gregg (1986), Convectively driven turbulent mixing in the upper ocean, *J. Phys. Oceanogr.*, *16*, 1777–1798.
- Skillingstad, E. D., and D. W. Denbo (1995), An ocean large-eddy simulation of Langmuir circulations and convection in the surface mixed layer, *J. Geophys. Res.*, *100*(C5), 8501–8522, doi:10.1029/94JC03202.

- Skylvingstad, E. D., W. D. Smyth, J. N. Moum, and H. Wijesekera (1999), Upper ocean turbulence during a westerly wind burst: A comparison of large-eddy simulation results and microstructure measurements, *J. Phys. Oceanogr.*, *29*, 5–28.
- Skylvingstad, E. D., W. D. Smyth, and G. B. Crawford (2000), Resonant wind-driven mixing in the ocean boundary layer, *J. Phys. Oceanogr.*, *30*, 1866–90.
- Smith, J. A. (1992), Observed growth of Langmuir circulation, *J. Geophys. Res.*, *97*, 5651–5664, doi:10.1029/91JC03118.
- Sullivan, P. P., J. C. McWilliams, and W. K. Melville (2007), Surface gravity wave effects in the oceanic boundary layer: Large-eddy simulation with vortex force and stochastic breakers, *J. Fluid Mech.*, *593*, 405–52.
- Sundermeyer, M. A., E. A. Terray, J. R. Ledwell, A. G. Cunningham, P. E. LaRocque, J. Banic, and W. J. Lillycrop (2007), Three-dimensional mapping of fluorescent dye using a scanning, depth-resolving airborne lidar, *J. Atmos. Oceanic Tech.*, *24*, 1,050–1,065.
- Terray, E. A., J. R. Ledwell, M. A. Sundermeyer, T. Donoghue, S. Bohra, A. G. Cunningham, P. E. LaRocque, J. Banic, W. J. Lillycrop, and C. E. Wiggins (2005), Airborne fluorescence imaging of the ocean mixed layer, in *Proc. IEEE/OES 8th Working Conf. on Current Meas. Technol.*, Southampton, U. K., IEEE, New York.
- Thorpe, S. A. (2004), Langmuir circulation, *Annu. Rev. Fluid Mech.*, *36*, 55–79.
- Van Roekel, L. P., B. Fox-Kemper, P. P. Sullivan, P. E. Hamlington, and S. R. Haney (2012), The form and orientation of Langmuir cells for misaligned winds and waves, *J. Geophys. Res.*, *117*, C05001, doi:10.1029/2011JC007516.
- Weller, R. A., J. P. Dean, J. F. Price, E. A. Francis, J. Marra, and D. C. Boardman (1985), Three-dimensional flow in the upper ocean, *Science*, *227*(4694), 1552–1556.